UV Resonance Raman and Excited-State Relaxation Rate Studies of Hemoglobin†

Namjun Cho, Sunho Song,‡ and Sanford A. Asher*

Department of Chemistry, University of Pittsburgh, Pittsburgh, Pennsylvania 15260

Received December 2, 1993; Revised Manuscript Received March 21, 1994®

ABSTRACT: We have measured the UV resonance Raman (UVRR) spectra of human methemoglobin fluoride (metHbF) and examined the Raman saturation behavior of the metHbF tryptophyl (Trp) and tyrosyl (Tyr) residues. Our high-quality UVRR spectra devoid of Raman saturation with 229- and 238.3-nm CW laser excitation allow us to determine small changes in Trp and Tyr residue Raman band frequencies and intensities caused by the hemoglobin R–T quaternary structural change induced by the allosteric effector inositol hexaphosphate. At 238.3-nm excitation, we observe a *ca.* 15 and 8% intensity increase for the Trp and Tyr bands, respectively, upon the R–T transition. In contrast, a small intensity decrease is observed with 225-nm excitation. These intensity alterations result from Trp and Tyr absorption and Raman excitation profile red-shifts which correlate with a strong 231.5-nm R–T absorption spectral change. These absorption and Raman excitation profile red-shifts and our model compound absorption studies together suggest a T-state increase in the hydrogen bond donation of the Trp-$\beta_2$37 and Tyr-$\alpha_1$42 residues at the $\alpha_1\beta_2$ subunit interface. The Tyr-α42 residue appears to be a hydrogen bond donor, rather than an acceptor. We determined the electronic excited-state relaxation rates of the Trp and Tyr residues in hemoglobin by using Raman saturation spectroscopy with 225-nm pulsed laser excitation. The observed average excited-state relaxation rate of the Trp residues is *ca.* 1/120 ps and is independent of the quaternary structure. This rate is slower than that observed for Trp residues of horse myoglobin. The average excited-state relaxation rate of the Tyr residues is *ca.* 1/60 ps for both the R and T quaternary forms. These are the first Tyr relaxation rates measured for any heme protein.

A detailed understanding of the hemoglobin cooperativity mechanism on a molecular level remains elusive in spite of the fact that more experimental data exist for this protein than for any other protein (Antonini & Brunori, 1971; Baldwin, 1975; Fermi & Perutz, 1977; Perutz, 1979; Asher, 1981; Dickerson & Geis, 1983; Rousseau & Ondrias, 1983; Perutz et al., 1987; Rousseau & Friedman, 1988). Alterations in the heme ligand affinity derive from tertiary and quaternary protein structural alterations which affect the heme ligand geometry and determine the energetics of ligand binding (Antonini & Brunori, 1971; Perutz et al., 1974a,b,c, 1978, 1987; Baldwin, 1975; Fermi & Perutz, 1977; Perutz, 1979; Asher, 1981; Asher et al., 1981; Dickerson & Geis, 1983; Rousseau & Ondrias, 1983; Henry et al., 1985; Rousseau & Friedman, 1988). The information transfer controlling the ligand affinity must obviously occur across the hemoglobin subunit interfaces. However, despite the numerous X-ray diffraction (Fermi & Perutz, 1977; Dickerson & Geis, 1983), UV–visible absorption (Perutz et al., 1974a,b,c, 1978; Asher et al., 1981; Henry et al., 1985), NMR (Perutz et al., 1974a,b, 1978; Viggiano & Ho, 1979), fluorescence (Hirsch et al., 1980; Hirsch & Nagel, 1981; Itoh et al., 1981; Szabo et al., 1984, 1989; Bucci et al., 1988a,b), and heme Raman spectroscopic studies (Spiro & Strekas, 1974; Asher et al., 1977, 1981; Asher, 1981; Asher & Schuster, 1981; Rousseau & Ondrias, 1983; Henry et al., 1985; Dasgupta et al., 1986; Rousseau & Friedman, 1988; Noble et al., 1989), the important structural changes that link protein tertiary and quaternary alterations to heme structural changes remain ambiguous.

Recent advances in Raman spectroscopy now allow excitation in the UV spectral region to permit the selective study of aromatic amino acids in peptides and proteins (Johnson et al., 1984; Copeland et al., 1985; Asher, 1988; Su et al., 1989; Kaminaka et al., 1990; Asher et al., 1991; Sweeney et al., 1991). This permits the selective study of the role of aromatic amino acids in the hemoglobin cooperativity mechanism through examination of both the static and dynamic structures and environments of aromatic amino acid residues (Copeland et al., 1985; Harada et al., 1986; Song & Asher, 1989; Su et al., 1989; Kaminaka et al., 1990, 1992; Spiro et al., 1990; Song et al., 1991; Rodgers et al., 1992; Jayaraman et al., 1993). In addition, the protein secondary structure can be studied by examining the peptide backbone vibrational spectra through excitation into the *ca.* 200-nm peptide $\pi \rightarrow \pi^*$ electronic transitions (Harada et al., 1986; Song & Asher, 1989; Spiro et al., 1990; Song et al., 1991). Furthermore, the recently developed technique of resonance Raman saturation spectroscopy (Teraoka et al., 1990; Harmon et al., 1990; Sweeney et al., 1991; Cho & Asher, 1993) which measures the ground-state recovery rate for an excited-state species conveys important protein structural information.

In the work discussed here, we utilize UV resonance Raman spectroscopy and UV resonance Raman saturation spectroscopy to examine changes in the environments of the tryptophyl (Trp) and tyrosyl (Tyr) residues of human methemoglobin fluoride (metHbF) upon protein R–T quaternary structural changes. We alter the protein quaternary conformation by using the allosteric effector inositol hexaphosphate (IHP). The metHbF quaternary R structure is very similar to that of the liganded ferrous derivative of hemoglobin. The T structure of metHbF, formed in the presence of inositol hexaphosphate, is very similar to that of deoxyHb (Fermi & Perutz, 1977; Deatherage et al., 1976). The resulting structural changes associated with the R–T quaternary

† Supported by NIH Grant 1R01GM30741-12.
* Author to whom correspondence should be addressed.
‡ Present address: Department of Chemistry, College of Science, Han Nam University, Ojung-Dong Daeduk-Ku, Taejon 300-791, South Korea.
® Abstract published in *Advance ACS Abstracts,* April 15, 1994.

0006-2960/94/0433-5932$04.50/0

structural transition, which have been previously well characterized, result in alterations in sulfhydryl group reactivity and UV–visible absorption and proton NMR spectroscopic changes (Perutz et al., 1974a,b,c, 1978).

Spiro and co-workers recently also reported the T–R difference Raman features for Trp and Tyr residues of deoxyHb and HbCO (Rodgers et al., 1992) and of metHbF (Jayaraman et al., 1993). Their studies proposed that Tyr-α42 accepts a hydrogen bond from protonated Asp-β99 in the T state. In contrast, our studies here suggests that the Tyr-α42 residue donates a hydrogen bond rather than accepts it. We observe concerted alterations in the Raman cross sections of Tyr and Trp residues upon metHbF quaternary structural changes. However, no significant alterations are evident in the relaxation rates of the Tyr and Trp residues in human metHbF between the R and T states. We interpret these results in terms of changes in the environments of particular Tyr and Trp residues.

EXPERIMENTAL PROCEDURES

N-Acetyl-L-tryptophanamide (NATRPA) was purchased from Sigma Chemical Co. *N*-Acetyl-L-tyrosine methyl ester (NATYR-OMe) and *N*-acetyl-L-tryptophan methyl ester (NATRP-OMe) were prepared by addition of their *N*-acetyl forms (Sigma Chemical Co.) to freshly prepared sodium methoxide in excess methanol. The identity and purity of the products were confirmed by proton NMR. Human hemoglobin (Hb) was obtained from Sigma Chemical Co. Stock solutions were filtered before use. Methemoglobin (metHb) was prepared by adding excess potassium ferricyanide to aqueous solutions of Hb. Excess oxidant was removed by extensive dialysis against deionized water. The solutions were centrifuged before use. Methemoglobin fluoride (metHbF) was prepared by adding metHb to 0.1 M NaF in 0.1 M sodium cacodylate at pH 7.0. In order to accomplish the R–T conversion of metHbF, a 10-fold excess of inositol hexaphosphate (IHP) relative to heme concentration was added to the metHbF solution. The hemoglobin sample concentrations were determined from the UV–visible absorbance of the metHbF heme Soret band (ϵ = 119 mM^{-1} cm^{-1}) (Perutz et al., 1974c). The solution concentrations for the Raman measurements were *ca.* 250 μM in heme. The solution pH was maintained at pH 7.0 with 0.1 M sodium cacodylate buffer.

We compared the IHP-induced absorption difference spectrum of HbF at a concentration of 0.25 mM in heme, as used for our Raman measurements, to that at 1.0 mM heme to examine the role of the dimer–tetramer equilibrium in determining the protein spectral changes. Because the absorption difference spectra at these concentrations are identical and because the dimer–tetramer equilibrium is known to be unimportant at 1 mM (Rodgers et al., 1992), we conclude that our measured spectral differences result only from the quaternary R to T structural transition.

The instrumentation used for Raman measurements is described in detail elsewhere (Asher et al., 1983, 1993; Jones et al., 1987). A Coherent Innova 300 intracavity frequency-double Ar^+-ion laser was used for 229- and 238.3-nm excitations. The 457.9- and 476.5-nm Ar^+-ion lasing lines were frequency-doubled with a β-barium borate doubling crystal to give 229 and 238.3 nm, respectively (Asher et al., 1993). A Lambda Physik Model EMG 103 Excimer laser operated at 200 Hz with a *ca.* 16-ns pulse width was utilized for low pulse energy flux 225-nm excitation. The 308-nm XeCl fundamental was used to pump a Lambda Physik FL 3002 dye laser. The dye laser output was frequency-doubled with a β-barium borate doubling crystal to yield 225-nm excitation. The excitation beam was defocused to yield a *ca.* 1-mm diameter at the sample. Higher pulse energy flux excitation at 225 nm utilized a Quanta Ray Nd-YAG laser operated at 20 Hz (pulse width *ca.* 4 ns). The 225-nm excitation frequencies were generated by mixing the doubled dye output with the YAG fundamental using KDP doubling and mixing crystals. The higher pulse energy flux excitation beam was defocused to yield a *ca.* 1-mm beam diameter at the sample.

We used a wire-guided jet sampling system similar to that of Kaminaka et al. (1992). We were unable to flow the sample in a quartz capillary or use a spinning cell because metHbF photoaggregates with UV excitation and precipitates at the spot illuminated by the focused laser beam. The sample solutions (200 mL) were recirculated at room temperature by gravity flow from a reservoir and by using a peristaltic pump to pump the solution back into the reservoir. The flow rates were sufficient to supply new sample to the illuminated volume between 200-Hz laser pulses. Samples were replaced after 20 min of exposure to the UV radiation. Two or three Raman spectra were summed to improve signal-to-noise. Sample absorption spectra were measured before and after each UV Raman experiment by using a Perkin-Elmer Model Lambda 9 UV–VIS–NIR spectrophotometer to ensure that no irreversible photodegradation occurred. Pulse energies were measured with a Scientech Model 361 power meter. The various pulse energy fluxes were obtained by placing neutral density filters in the beam path prior to the sample. The Raman scattered light was collected using a 150° backscattering geometry, dispersed by a Spex Triplemate spectrometer with 1800 groove/mm grating and detected by using a PAR OMA III detection system with a UV-enhanced intensified Reticon detector.

Sodium cacodylate buffer was utilized as an internal intensity standard. The absolute Raman cross section of the 607-cm^{-1} mode, which is a symmetric As–C stretching vibration, was previously determined by Song and Asher (1991). Furthermore, cacodylic acid shows no Raman saturation under our experimental conditions. The absolute Raman cross sections were determined from the relative peak height ratio of the sample bands to that of the 607-cm^{-1} cacodylic acid band. The relative ratios were corrected using the measured spectrometer throughput efficiency and the response sensitivity of individual detector pixel elements.

The Raman intensities measured for the protein samples depend upon the incident pulse energy flux, the absorption cross section, and the rate of repopulation of the ground state from excited-state species formed due to photon absorption. Raman saturation spectroscopy utilizes this dependence of the Raman intensities upon the incident pulse energy flux to determine the ground-state repopulation rate, $1/T_1$ (Teraoka et al., 1990; Harmon et al., 1990); since all excited-state species relax to the ground state in Hb, the reciprocal of T_1 is the excited-state relaxation rate. We utilized the Raman saturation methodologies described by Teraoka et al. (1990) and Harmon et al. (1990) and utilized the *BMDP 3R* nonlinear least-squares regression programs for determining the lifetime values and their estimated standard deviations.

RESULTS

Figure 1 shows the absorption spectrum of metHbF at pH 7.0 and the absorption difference spectrum of metHbF in the presence and absence of the allosteric effector inositol hexaphosphate (IHP) which converts the R state to the T state. The numerous bands between 350 and 700 nm in the metHbF absorption spectrum derive from heme electronic

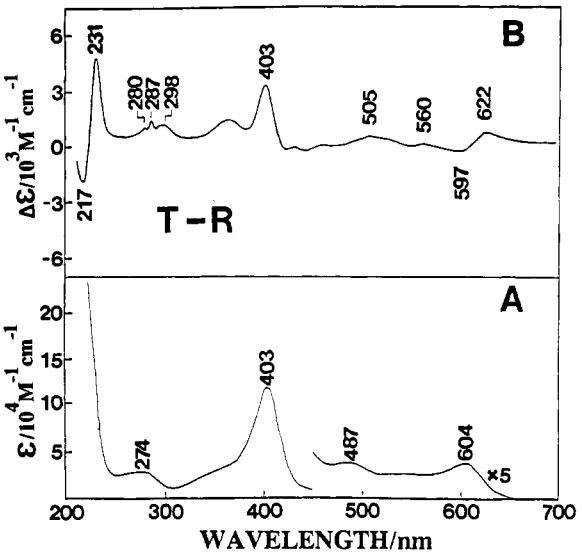

FIGURE 1: (A) Absorption spectrum of 250 μM (heme concentration) methemoglobin fluoride (metHbF) in 0.1 M cacodylic acid at pH 7.0. (B) Difference absorption spectrum of metHbF in the presence and absence of inositol hexaphosphate (IHP).

transitions. The 403-nm Soret band results from an in-plane heme π–π^* electronic transition, while the 480–700-nm bands derive from both π–π^* electronic transitions and charge-transfer transitions (Eaton & Hochstrasser, 1970; Smith & Williams, 1970; Perutz et al., 1974a; Asher et al., 1981). The broad features between 250 and 300 nm have contributions from the $L_b \leftarrow A_{1g}$ π–π^* electronic transition of tyrosine and the $L_a/L_b \leftarrow A_{1g}$ π–π^* transitions of tryptophan and contain a small contribution from the $L_b \leftarrow A_{1g}$ π–π^* transition of phenylalanine (Perutz et al., 1974b,c, 1978). The sharp absorbance increase below 240 nm in due to strong Tyr, Trp, and Phe electronic transitions with a strong contribution below 220 nm from the peptide backbone π–π^* transitions.

The heme absorption difference spectrum (Figure 1B) shows a red-shift of the charge-transfer band near 600 nm and a slight absorbance increase of the Soret band upon formation of the T state. Aromatic amino acid absorption changes due to hemoglobin tertiary and quaternary protein structural changes have been previously assigned in the 270–320-nm region to environmental changes of Tyr and Trp at the $\alpha_1\beta_2$ subunit interface (Perutz et al., 1974b,c). The broad feature at *ca.* 300 nm has been suggested to result from changes in the hydrogen bonding of Trp-$\beta_2$37 (Perutz et al., 1974b), and the sharp features at 280 and 287 nm have been suggested to derive from decreased interactions between Tyr-$\alpha_1$42 and the guanidinium group of Arg-$\beta_2$40 (Perutz et al., 1974a,b) based upon absorption, circular dichroism, and NMR studies of mutant hemoglobins and hemoglobin derivatives (Perutz et al., 1974b, 1978). However, Baldwin and Chothia (1979) reported that the guanidinium group of Arg-β40 contacts the phenyl ring of Tyr-α42 in *both* the R and T states. These absorption difference features may instead result from a change in the hydrogen bonding of Tyr-α42 to Asp-β99; the Tyr-α42 H-bond to Asp-β99 in the T state appears broken in the R state (Baldwin & Chothia, 1979).

The strong protein absorption near 225 nm derives primarily from the $L_a \leftarrow A_{1g}$ transition of Tyr and the $B_b \leftarrow A_{1g}$ transition of Trp, with little contributions of cysteine and peptide backbone transitions (Bailey et al., 1968; Demchenko, 1981). Trp and Tyr absorption spectral changes in the 210–240-nm spectral region have been demonstrated to correlate directly with the *ca.* 270–300-nm spectral changes (Bailey et al., 1968; Sweeney et al., 1991). Thus, the observed HbF absorption

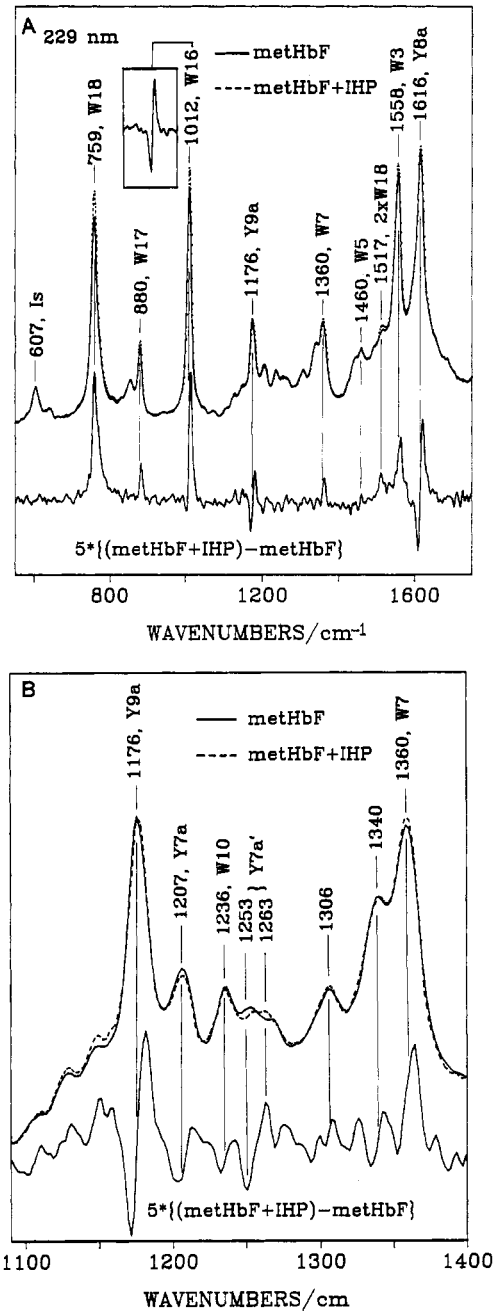

FIGURE 2: 229-nm excited UV resonance Raman spectra of 250 μM (heme concentration) metHbF (—) and metHbF+IHP (- - -) and the difference spectrum of metHbF+IHP minus metHbF (bottom) at pH 7.0 with a power flux of 2.9 W/cm² using CW laser excitation. The slit width used resulted in a *ca.* 8.7-cm⁻¹ spectral band-pass. The 607-cm⁻¹ band derives from the cacodylic acid internal standard Accumulation time is 15 min. (A) 550–1750 cm⁻¹. The inset shows the calculated difference spectrum of the Trp 1012-cm⁻¹ band, where the spectra were normalized, such that the 1012-cm⁻¹ band intensities were identical in order to show the frequency shift. (B) Expanded view of the 1100–1400-cm⁻¹ region.

difference maximum at 231.5 nm is related to the difference features observed between 270 and 320 nm which have been previously assigned to Tyr and Trp changes at the $\alpha_1\beta_2$ subunit interface.

Figure 2A shows the 229-nm excited resonance Raman spectra of metHbF and metHbF+IHP solutions containing 0.1 M sodium cacodylate at pH 7.0 and the metHbF+IHP minus metHbF difference spectrum. The internal intensity standard band at 607 cm⁻¹, which is used to normalize the spectra for subtraction, derives from the symmetric As–C stretching mode of the cacodylate buffer (Song & Asher,

Table 1: Assignment of Strongly Enhanced MetHbF Bands with 238.3-, 229-, and 225-nm Excitation[a]

cm^{-1}	band	assignment
1616	Tyr Y8a	in-plane ring stretching
1558	Trp W3	C_2–C_3 stretching mode of pyrrole ring
1360	Trp W7	Fermi resonance between N_1–C_8 stretching in pyrrole ring and
1340		combination bands of out-of-plane bending
1276		CH_3 deformation of cacodylic acid
1236	Trp W10	mixed mode of CH bending and C_3–C_3 stretching
1207	Tyr Y7a	ring C–C_β stretching
1176	Tyr Y9a	in-plane C–H bending
1012	Trp W16	symmetric benzene/pyrrole out-of-phase breathing mode
880	Trp W17	indole ring vibration with N–H bending
855	Tyr 2Y16a+Y1	Fermi resonance involving symmetric ring stretching mode
833		
759	Trp W18	symmetric benzene/pyrrole in-phase breathing mode
607		cacodylic acid As–C stretching

[a] See Johnson et al. (1986) and Harada and Takeuchi (1986).

Table 2: Raman Cross Section per Aromatic Amino Acid Residue for MetHbF and MetHbF + IHP in 0.1 M Cacodylic Acid at pH 7.0 for 229- and 225-nm Excitation[a]

		238.33 nm		229 nm		225 nm	
	cm^{-1}	metHbF R	metHbF+IHP T	metHbF R	metHbF+IHP T	metHbF R	metHbF+IHP T
Trp	759	0.100	0.118	2.18	2.47	1.82	1.73
Trp	1012	0.146	0.168	2.25	2.43	2.00	1.90
Trp	1360	0.114	0.124	0.750	0.773	0.986	0.931
Trp	1558	0.257	0.284	1.97	2.16	2.76	2.66
Tyr	1616	0.333	0.362	1.11	1.12	1.33	1.42

[a] Units: barns per molc-sr.

1991). The Raman spectra are dominated by symmetric ring modes of Tyr and Trp whose assignments are listed in Table 1. Converting the quaternary structure of metHbF from the R to T state with IHP results in an increased intensity for almost all of the Trp bands. The Trp bands at 759 cm^{-1} (W18) and 880 cm^{-1} (W17) show 12% and 9% intensity increases without any observed frequency shifts, while the Trp W16 band at 1012 cm^{-1} shows both a 7% intensity increase and a *ca.* 0.5-cm^{-1} frequency increase (most easily observed in the inset). The 1517-cm^{-1} band, which was assigned as the overtone of the 759-cm^{-1} Trp W18 mode (Rodgers et al., 1992), shows the largest **relative** intensity change. The Tyr Y8a band at 1616 cm^{-1} shows a *ca.* 1.5-cm^{-1} frequency upshift with little or no intensity change. The measured Raman cross sections are listed in Table 2.

These metHbF and metHbF+IHP spectra and their difference spectrum are very similar to the recently published 230-nm excited UVRR spectra of Jayaraman et al. (1993) and are also similar to the 230-nm excited UVRR spectra of HbCO and deoxyHb and the deoxyHb – HbCO difference spectrum by Rodgers et al. (1992) except in the Trp W3 band region. The Trp W3 band appears at 1558 cm^{-1} with a very slight shoulder at 1549 cm^{-1}. Rodgers et al. assigned a much more obvious shoulder in oxy- and deoxyHb to the Trp-β37 residue based on their UVRR spectrum of a natural mutant hemoglobin, Hb Rothschild, in which Trp-β37 is replaced by Arg. They reported that the 1549-cm^{-1} Trp-β37 W3 band shows a 37% greater intensity in deoxyHb than in HbCO, while the overlapped W3 bands contributed by Trp-α14 and -β15 at *ca.* 1558 cm^{-1} show no intensity changes. In contrast, our 229-nm difference spectrum of metHbF+IHP minus metHbF shows similar increased intensities for both the 1549-cm^{-1} shoulder and the 1558-cm^{-1} W3 bands. The Trp W18 band at 759 cm^{-1}, which was not shown in their spectrum, shows an intensity increase of *ca.* 12%. Although Copeland et al. (1985) reported a 4-cm^{-1} downshift of this band in HbF for 218-nm excitation upon addition of IHP, we observe no frequency shift for this band.

Figure 2B shows an expanded view of the 1100–1400-cm^{-1} region. The Tyr Y9a band at 1176 cm^{-1} shows a *ca.* 1-cm^{-1} upshift with little intensity change. The weak and broad Tyr Y7a′ band around 1260 cm^{-1} is sensitive to the hydrogen-bonding state of the Tyr phenol OH group (Takeuchi et al., 1989). The broad contour of this band probably derives from the overlap of the different hydrogen-bonding states of the different Tyr residues in hemoglobin. The 1253-cm^{-1} shoulder of this band shifts to 1263 cm^{-1} upon the R to T transition. The increased intensity at 1263 cm^{-1} indicates that at least one out of the six inequivalent Tyr residues becomes more of a hydrogen bond donor in the T state (Takeuchi et al., 1989). The Fermi resonance doublet Trp W7 bands at around 1340–1360 cm^{-1} (Harada et al., 1986) show a small relative intensity increase of the 1360-cm^{-1} component compared to that at 1340 cm^{-1}.

Figure 3 shows the 238.3-nm excited resonance Raman spectra of metHbF and MetHbF+IHP and the difference spectrum between metHbF+IHP and metHbF. All of the Tyr and Trp bands show increased intensities in the T state. The Tyr Y8a and Y9a bands are strongly enhanced, relative to Trp bands, at this excitation wavelength. The strongly enhanced Tyr Y8a band at 1616 cm^{-1} and the Y9a band at 1176 cm^{-1} show *ca.* 8% and *ca.* 6% intensity increases, respectively. The Trp W16 band at 1012 cm^{-1} shows a ca. 15% intensity increase. These 238-nm excitation Raman intensity increases probably derive from the absorption band red-shift observed in Figure 1 (vide infra). This absorption red-shift may result either from changes in the Tyr and Trp hydrogen-bonding states or from alterations in the environments of the Tyr and Trp residues.

Figure 4 shows the 225-nm excited UVRR spectra of metHbF and metHbF+IHP excited at low pulse energy flux values. The spectra are similar to those of Figure 2; the dominant bands derive from Trp and Tyr residues, and the contribution of phenylalanine is less than 5% based upon its measured Raman cross section (Johnson et al., 1986); 225-nm excitation increases the Trp band intensities relative to

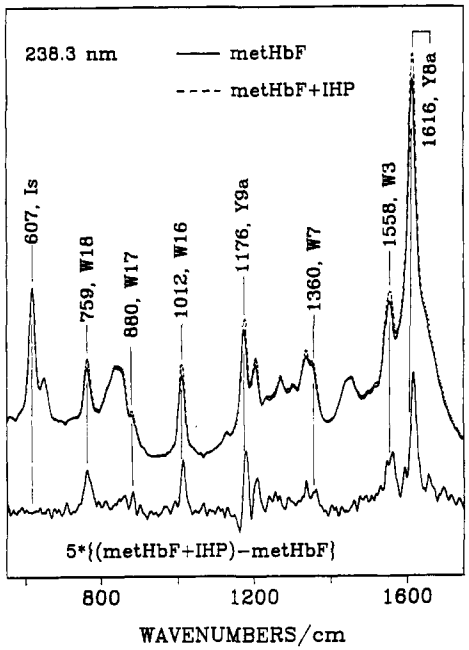

FIGURE 3: 238.3-nm excited Raman spectra of 250 μM (heme concentration) metHbF (—) and metHbF+IHP (- - -) at pH 7.0 with a CW laser power flux of 6.4 W/cm^2. The slit width used resulted in a *ca.* 12-cm^{-1} spectral band-pass. Accumulation time is 15 min.

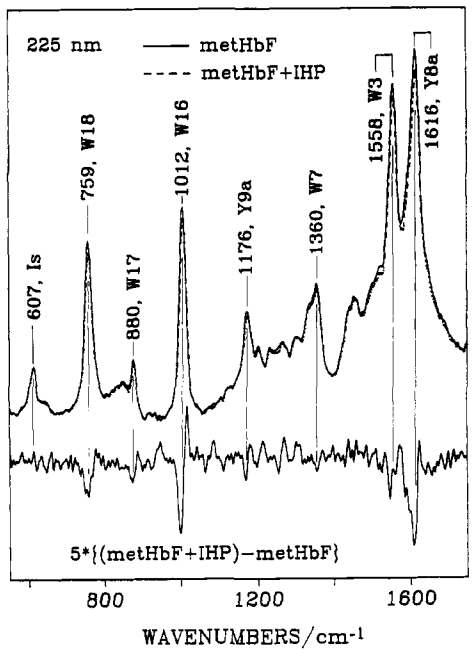

FIGURE 4: 225-nm excited Raman spectra of 250 μM metHbF (—) and metHbF+IHP (- - -) at pH 7 with a pulse energy flux density of 3 mJ/cm^2 by using an excimer laser with a pulse length of *ca.* 15 ns. The slit width used resulted in a *ca.* 18-cm^{-1} spectral band-pass. Accumulation time is 15 min.

Tyr because 225-nm excitation is closer to the Trp excitation profile maximum (Sweeney & Asher, 1990) than to that of Tyr (Ludwig & Asher, 1988). In contrast to the increased T-state Trp and Tyr cross sections observed with 238-nm excitation, 225-nm excitation results in a *ca.* 4% decrease in the average T-state Raman cross section for Trp and a *ca.* 6% decreased cross section for Tyr (Table 2). The spectra also show frequency shifts similar to those observed with 229-nm excitation (Figure 2). The difference spectrum clearly shows the frequency shift of the 1012-cm^{-1} Trp W16 band.

Figure 5 compares the ±IHP difference spectra for the three different excitation wavelengths. The relative contribu-

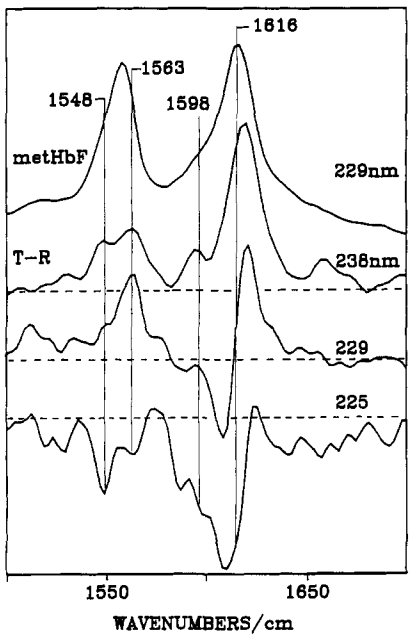

FIGURE 5: Comparison of the difference spectra between the different excitation wavelengths. Also shown are the 229-nm Raman spectra of metHbF.

tion of the 1548- and 1563-cm^{-1} components of the W3 band differs between these excitation wavelengths. The difference feature at 1548 cm^{-1}, which Rodgers et al. (1992) assigned to Trp-β37, shows a dominating trough at 225-nm excitation, shows a small peak at 229-nm excitation, and shows a clear positive shoulder for 238-nm excitation.

These relative Raman cross-section changes with 225-, 229-, and 238.3-nm excitation are exactly those expected from absorption and Raman excitation profile red-shifts of the Trp and Tyr residues. For example, the Trp 1012-cm^{-1} band intensity decreases by 4% at 225 nm, but increases by 7% and 15% at 229 and 238.3 nm, respectively. The Tyr 1616-cm^{-1} band intensity decreases 6% for 225-nm excitation and stays constant at 229-nm excitation, but increases by 8% with 238.3-nm excitation.

Figure 6 shows the absorption spectra of Trp and Tyr, as well as the absorption difference spectrum which would result from a 2-nm absorption red-shift. We also plot the **relative** absorption difference spectrum obtained by dividing the difference spectrum by the original absorption spectrum.

For Trp in water, the maximum absorbance occurs at 220 nm, but this maximum would be expected to red-shift by 4 nm in the hydrophobic protein environment (Sweeney & Asher, 1990; Sweeney et al., 1991). The absorption difference peak for a 2-nm absorption band shift occurs at *ca.* 227.5 nm, which is 7.5-nm red-shifted from the absorption maximum at 220 nm. In a protein, this peak would be expected to occur at 231.5 nm, close to the 231-nm peak, experimentally observed in Figure 1. The peak is also expected to be asymmetric in a manner similar to that observed in Figure 1; the absorbance difference peak on the red side should be much larger than the absorption trough on the blue side. At this point, we can only estimate the relative spectral change which one Tyr and one Trp residue could contribute to give rise to the 231.5- and 280–300-nm absorption spectral features. The absorption difference spectrum can be very roughly approximated if a Trp and a Tyr each red-shifts by 2 nm.

Figure 6 also shows the Raman excitation profile of the 1012-cm^{-1} band of Trp in water taken from the results of Sweeney and Asher (1990), and the excitation profile of the 1616-cm^{-1} band of Tyr in water taken from the results of

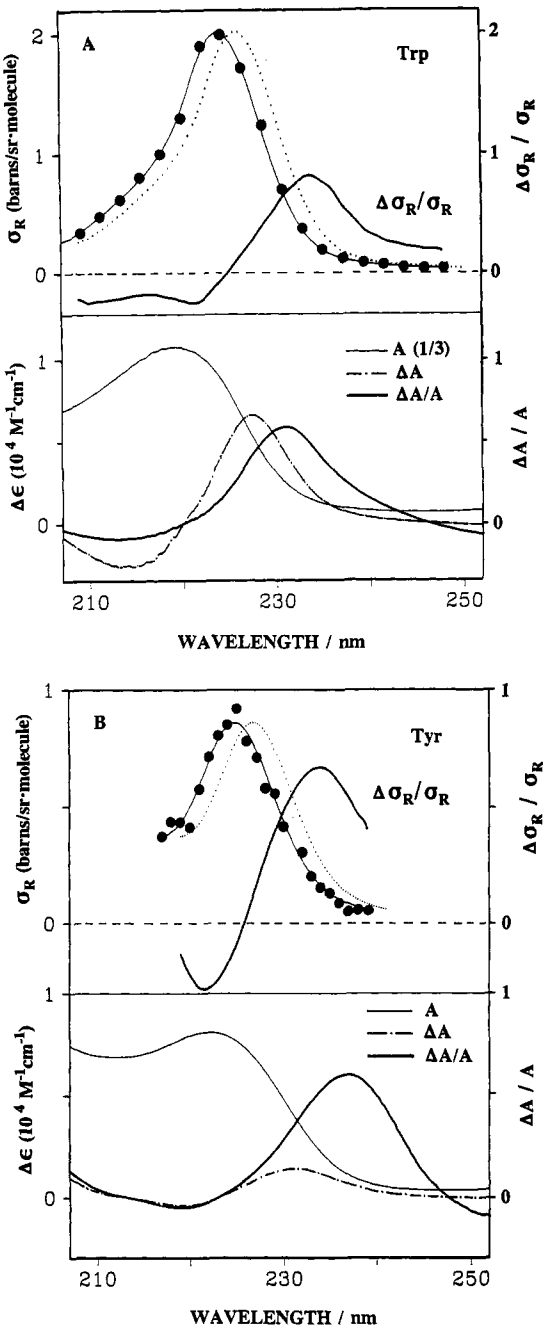

FIGURE 6: Absorption spectral shifts and Raman excitation profile shifts for Trp and Tyr. Bottom panels show the absorption spectra (—) and the absorption difference spectra (– · –) observed for a rigid 2-nm absorption spectral red-shift. Also shown is the calculated relative absorption difference spectrum, $\Delta A/A$ (thick solid curve). The top panel shows the Raman excitation profile (·—·) (Sweeney & Asher, 1990; Ludwig & Asher, 1988) and the calculated relative Raman cross-section change, $\Delta\sigma_R/\sigma_R$ (—), upon a 2-nm excitation profile red-shift (···). (A) For Trp; (B) for Tyr.

Ludwig and Asher (1988). Figure 6 also shows the calculated **relative** Raman cross-section changes that would result from a shift of each Raman excitation profile by 2 nm.

The Raman excitation profile maximum of aqueous Trp red-shifts by 4 nm from the absorption maximum and occurs at 224 nm (Sweeney & Asher, 1990). The excitation profile maximum would occur at *ca.* 228 nm in a protein environment. Figure 6 indicates that if a 2-nm red-shift occurred for the Raman excitation profile of Trp in water, the **relative** Raman excitation profile would show a maximum **relative** cross-section increase of *ca.* 80%, which would occur at 234 nm. For Trp in a protein, this would occur at 238 nm.

We observe a 15% increased 1012-cm^{-1} Trp band intensity for 238.3-nm excitation. If this intensity increase resulted from only the single Trp-β37 residue at the $\alpha_1\beta_2$ subunit interface (and if its Raman cross section were initially identical to that of the average Trp cross section in the R state), the Raman cross section of this Trp-β37 in the T state would have increased by 45%. Further, if as suggested by Jayaraman et al. (1993) IHP addition only converts 66% of the R state to the T state, this Trp-β37 residue at the $\alpha_1\beta_2$ interface would have increased its cross section by 68%. This is close to that which would be expected for an excitation profile red-shift of 2 nm for a single Trp residue.

The W3 intensity alterations indicated in Figure 5 suggest that the 1548-cm^{-1} shoulder component assigned to the Trp-β37 residue undergoes a larger absorption red-shift than the other Trp residues, which instead contribute to the main 1558-cm^{-1} peak. The fact that the 238-nm excitation Trp-β37 difference feature is as large as that of the sum of the other Trp residues suggests that it red-shifts more than the other Trp residues upon conversion to the T state (>2 nm, vide infra). This is consistent with it showing a dominating trough with 225-nm excitation.

The observed Trp Raman intensity changes for the main W3 peak at 1558 cm^{-1} are similar to those expected for a *ca.* 2-nm absorption red-shift. This red-shift should result in a large Raman intensity increase on the red edge of the excitation profile, with only a small decrease on the blue side. The magnitude will, of course, depend upon the exact spectral shift and, for proteins, will depend upon the number of residues which undergo this spectral change.

The situation is entirely analogous for the Tyr residues (Sweeney et al., 1991; Ludwig & Asher, 1988). The absorption maximum of Tyr in water occurs at 222 nm. A 2-nm absorption red-shift results in an absorption difference peak at 232 nm (Figure 6). The Raman excitation profile maximum of aqueous Tyr occurs at 225 nm, which is 3-nm red-shifted from the absorption maximum (Ludwig & Asher, 1988). The rigid 2-nm red-shift of this excitation profile would result in a maximum relative Raman cross-section increase of 67% at 234 nm. This maximum would occur at *ca.* 238 nm in a protein. If the Tyr intensity change upon the R–T transition of metHbF were only due to the Tyr-α42 residue (and if its Raman cross section in the R state were the same as the average Tyr cross section), our observed 8% intensity increase in the Tyr 1616-cm^{-1} band with 238.3-nm excitation would result from a 48% Raman cross-section increase of this Tyr-α42 residue. If there were only a 66% R to T conversion of metHbF by IHP, as mentioned above, the Raman cross section of this Tyr-α42 residue would have increased by 72% in the T state relative to that in the R state. This is similar to that expected to result from a 2-nm absorption red-shift. However, other Tyr residues may also contribute to the Raman intensity changes. [The possibility of the contribution of Tyr-α140 was also considered by Rodgers et al. (1992).]

Table 3, which illustrates the dependence of the Trp and Tyr absorption spectra upon the solvent environment, indicates that all of the Trp absorption bands red-shift as the hydrogen bonding accepting ability of the solvents increases according to the β-scale of solvent basicity (Kamlet et al., 1981). This correlation is not expected to be perfect because variations also occur for the solvent polarity and the H-bonding donation ability. However, our results indicate that a red shift of the Trp absorption spectrum correlates directly with an increase in Trp H-bonding donation.

We also examined the photochemical relaxation rates of the Trp and Tyr residues by measuring their resonance Raman

Table 3: Absorption Maxima of *N*-Acetyl-L-tyrosine Methyl Ester and *N*-Acetyl-L-tryptophan Methyl Ester[a]

	β[b]	NATYR-OMe[c]			NATRP-OMe[d]				NATRP-OEt[e]			indole		
cyclohexane	0.00											215.0	266.4	287.0
water	0.18	222.8	274.6	281.4	219.0	272.2	279.4	287.6	219	279.4	287.6			
acetonitrile	0.31	224.8	277.2	283.4	221.4	273.8	280.2	289.2						
ethyleneglycol	0.52	224.4	276.4	282.6	221.2	272.6	280.2	288.6						
methanol	0.62	225.4	277.6	284.2	220.0	274.2	281.0	289.6	220.8	280.8	289.6	216.4	271.0	287.2
ethanol	0.77	226.2	278.2	284.4	221.4	274.6	281.4	290.0						
2-propanol	0.95	226.2	278.2	284.6	221.4	275.0	281.8	290.2	221.2	281.6	290.0	217.0	271.8	287.4
cyclohexanol									222.8	282.4	290.6	218.4	272.4	288.2
triethylamine	0.71								*f*	282.4	291.2	*f*	272.8	288.4

[a] Units: nanometers. [b] β scale of solvent basicity (Kamlet et al., 1981). [c] *N*-Acetyl-L-tyrosine methyl ester [d] *N*-Acetyl-L-tryptophan methyl ester. [e] *N*-Acetyl-L-tryptophan ethyl ester. [f] Could not observe due to strong triethylamine absorption.

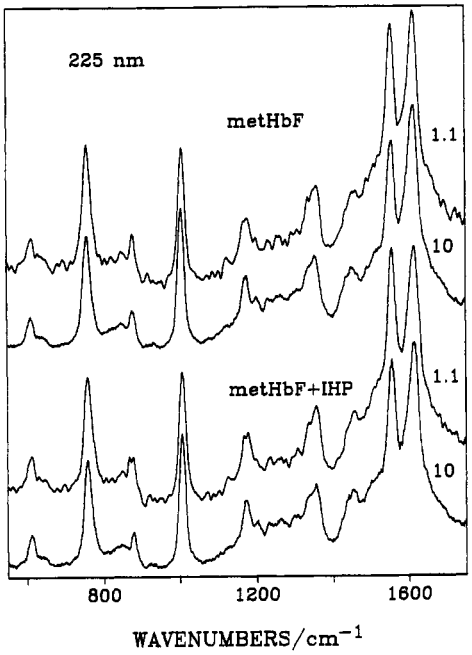

FIGURE 7: 225-nm excited Raman spectra of metHbF (top two spectra) and metHbF+IHP (bottom two spectra) at different pulse energy fluxes. Pulse energy flux values are indicated on the right side (mJ/cm²). Cacodylate intensities at 607 cm⁻¹ are normalized for direct comparison.

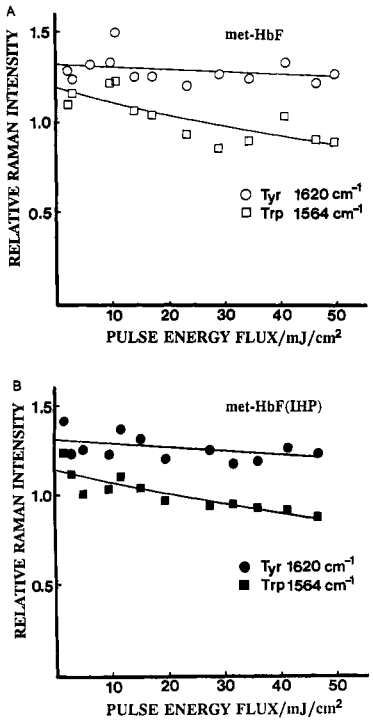

FIGURE 8: Plots of the metHbF 1558-cm⁻¹ Trp residue (□) and 1616-cm⁻¹ Tyr residue (○) intensities measured at 225-nm excitation relative to the internal intensity standard as a function of pulse energy flux. pH was maintained with 0.1 M cacodylic acid buffer at pH 7.0. Solid lines represent the nonlinear best-fitted curve using the Raman saturation model. See text for details. (A) Without IHP; (B) with IHP.

saturation curves in the presence and absence of IHP. Figure 7 show the 225-nm excited resonance Raman spectra of metHbF with and without IHP under various pulse energy flux excitations. At higher pulse energy fluxes, the Trp band intensities decrease significantly relative to both the internal standard and the 1616-cm⁻¹ Tyr band. For example, the relative intensity ratio of the 1558-cm⁻¹ Trp band to the 1616-cm⁻¹ Tyr band using 225-nm excitation is 0.96 at low pulse energy fluxes but decreases to 0.83 at high pulse energy fluxes. The decreased Trp to Tyr band intensity at high pulse energy flux values indicates a larger ground-state depletion for Trp compared to Tyr.

Figure 8 shows Raman saturation curves of the 1558-cm⁻¹ Trp and 1616-cm⁻¹ Tyr bands of metHbF with and without IHP relative to the internal standard 607-cm⁻¹ cacodylic acid band as a function of incident pulse energy flux. This saturation results from the depletion of Trp molecules in the ground state due to the significant population of excited electronic states at high pulse energy fluxes. In contrast to Trp, the 1616-cm⁻¹ Tyr band shows only a small decrease in its relative intensity with increasing pulse energy flux values. The observed saturation behavior of these bands appears independent of the presence of IHP. We determine a population-averaged T_1 lifetime of 120 ± 35 ps for Trp and 60 ± 40 ps for Tyr.

DISCUSSION

Conformational Dependence of Raman Intensities and Frequencies. The observed resonance Raman intensities for any excitation wavelength depend upon the Raman cross sections, the ground state-species concentration, and the incident laser power. The resonance Raman cross sections depend upon the electronic transition frequencies and moments, the Raman excitation profiles, and the refractive index of the medium, which determines the magnitude of the electric field around each protein residue (Albrecht, 1960; Albrecht & Hutley, 1971; Harmon & Asher, 1988, 1990; Larkin et al., 1991). The aromatic amino acid electronic transition moments and the resonant absorption frequencies, as well as the local refractive indexes, depend upon the protein conformation. Protein conformational changes modulate the local aromatic amino acid structure and environment by altering intramolecular interactions, such as hydrogen bonding, electrostatic interactions, and dispersive interactions between residues.

There are a total of 12 Tyr and 6 Trp residues in human hemoglobin: 3 Tyr each per α subunit and β subunit, 2 Trp

per β subunit, and 1 Trp per α subunit (Dickerson & Geis, 1983). The Trp-α14 and -β15 residues are located within the subunit interiors and are unlikely to be greatly affected by the hemoglobin R–T quaternary transition. The most structurally sensitive residue is likely to the Trp-β37 which occurs at the $\alpha_1\beta_2$ subunit interface and hydrogen-bonds to Asp-α94 in the T state. This Trp does not hydrogen-bond to Asp-α94 in the R state (Dickerson & Geis, 1983), but hydrogen-bonds to the Asn-β102 backbone carbonyl group. Among the six inequivalent Tyr residues in the $\alpha_1\beta_2$ subunit pair, the three Tyr-α24, Tyr-α35, and Tyr-β130 have no hydrogen bond partners, and their environments are not significantly changed by the R to T quaternary structure change. Tyr-$\alpha_1$140 and Tyr-$\beta_2$145 have hydrogen-bonding interactions with Val-α_1-93 and Val-$\beta_2$98 carbonyl groups, respectively, in both the R and T states. In contrast, Tyr-α42 hydrogen-bonds to the Asp-β99 carboxylate group in the T state, but not in the R state (Baldwin & Chothia, 1979; Shaanan, 1983). Thus, we expect most alterations in the UVRR spectra of the Tyr bands to derive from the Tyr-α42 residue.

The spectral alterations observed for metHbF between the R and T states appear to involve absorption and Raman excitation profile red-shifts and small Raman frequency increases for the Tyr Y7a′ contour and the Tyr Y9a and Y8a bands and the Trp W16 band in the T state. According to Rodgers et al. (1992), the Raman excitation profile of *p*-cresol red-shifts when it becomes more of an H-bond donor or becomes less of an H-bond acceptor. This conclusion is consistent with our examination of the dependence of the absorption spectra of Tyr derivatives on the solvent (Table 3). Our study indicates that an *increase* in the *solvent* H-bond acceptance ability or a *decrease* in the solvent H-bond donation ability red-shifts the Tyr and Trp absorption bands (Table 3). The absorption maxima of Tyr and Trp red-shift upon increasing the β scale of solvent hydrogen bond acceptor basicity, or upon decreasing the α scale of solvent hydrogen bond donor acidity in the order of water, acetonitrile, ethylene glycol, methanol, ethanol, and 2-propanol (Kamlet et al., 1981). As discussed above, the absorption difference spectrum in Figure 1 can be *roughly* modeled by rigidly shifting the absorption spectra of Trp and Tyr by 2 nm.

Our observed Raman excitation profile and absorption red-shifts strongly indicate that the Tyr-α42 becomes more of an H-bond donor and/or less of an H-bond acceptor in the T state (Figure 9). This result is consistent with the suggested formation of a Tyr-α42 hydrogen bond to Asp-β99 in the T state (Baldwin & Chothia, 1979). Additional confirming evidence comes from the observed Tyr Y7a′ band frequency increase. Takeuchi et al. (1989) report that the phenolic Y7a′ C–O stretching band frequency is especially sensitive to the H-bonding state of the Tyr phenolic OH group. Y7a′ appears at 1265–1275 cm^{-1} if the phenolic group is a hydrogen bond donor, while it downshifts to 1230–1240 cm^{-1} if, instead, the phenolic hydroxyl oxygen is a hydrogen bond acceptor. In contrast, the Y7a′ band occurs around 1255 cm^{-1} in weakly or non-hydrogen-bonded states. We observe that the broad 1260-cm^{-1} band contour in the R state shifts up *ca.* 10 cm^{-1} from 1253 to 1263 cm^{-1} in the T state. The breadth of the band obviously results from the contributions of the different H-bonded Tyr residues in metHbF; Tyr-α24, Tyr-α35, and Tyr-β130 do not appear to H-bond, while Tyr-α140 and Tyr-β145 appear to strongly H-bond (Baldwin & Chothia, 1979). The *ca.* 10-cm^{-1} upshift of part of this band probably reflects the alteration in the H-bonding state of the Tyr-$\alpha_1$42 at the $\alpha_1\beta_2$ interface.

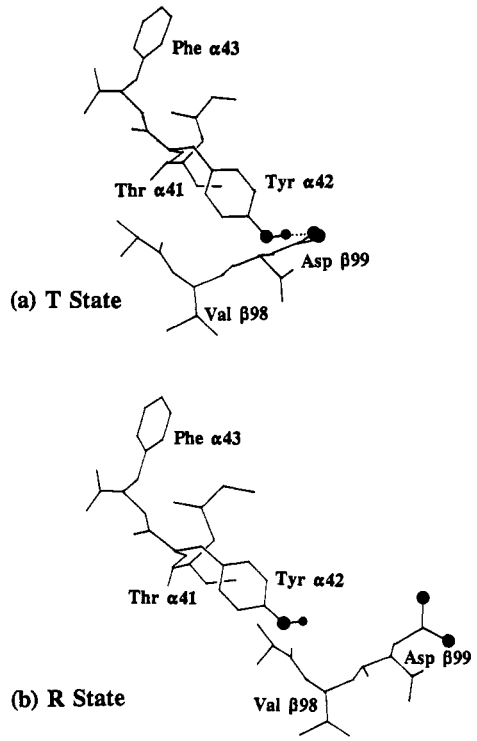

FIGURE 9: Schematic showing the hydrogen-bonding state of Tyr-α42 in the R and T states [adapted from Baldwin and Chothia (1979)].

Our conclusions that we spectrally detect the alteration of hydrogen bonding of Tyr-$\alpha_1$42 from being non-H-bonded in the R state to a H-bond donor in the T state are contrary to the recent study of Rodgers et al. (1992) which concluded that the Tyr-α42 residue is a hydrogen bond acceptor from Asp-β99 in T-state deoxyhemoglobin. Rodgers et al.'s conclusion is based on their observed frequency upshifts of *ca.* 1 and 1.8 cm^{-1} in Y8b and Y8a and from the 3% intensity loss in the Y8a band intensity with 230-nm excitation.

This disagreement in interpretation results from Rodgers et al.'s conclusion that the slight intensity decrease and the frequency increase of the Y8a band indicate an increased H-bonding acceptance of the Tyr residue (Rodgers et al., 1992). Rodgers et al.'s (1992) assumption that the Tyr Y8a intensity decrease with 230-nm excitation in deoxyHb is the result of a decreased H-bond donation or an increased H-bond acceptance is based on the ν8a Raman excitation profile of *p*-cresol which blue-shifts and shows an intensity decrease at 230 nm in trifluoroacetic acid, compared to that in cyclohexane. In contrast, the excitation profile red-shifts and shows a 230-nm intensity increase in tetrahexylammonium chloride. However, the observation of a Tyr Y8a band intensity decrease at only the single 230-nm excitation wavelength cannot actually determine whether the Raman excitation profile of the Tyr residue blue-shifts or red-shifts or undergoes a hypo- or hyperchromic shift. Figure 5 clearly demonstrates that the Raman excitation profile of the Tyr Y8a band red-shifts upon the R to T transition. Indeed, Jayaraman et al.'s (1993) study of metHbF with 219- and 230-nm excitation also suggests a red-shift. Our Raman excitation profile red-shift is clear evidence of an increased H-bond donation of the T-state Tyr residue, on the basis of both Rodgers et al.'s Raman excitation profile study of *p*-cresol and our study of the Tyr absorption dependence on solvent H-bond acceptance and our observed frequency alterations of the Y7a′ band.

Rodgers et al. also emphasize the correlation of the Y8a and Y8b band frequencies with solvent H-bond acceptance or donation. These correlations are based on solution studies

which found a strong frequency dependence of the Y8b band and a weak frequency dependence of the Y8a band on solvent. We were unable to determine the frequency dependence of the Y8b band due to the overlap with other bands. However, the extensive previous study by Tekeuchi et al. (1989) on well-defined hydrogen-bonded crystalline model compounds concluded that the Y8a and Y8b bands are not clear markers of the H-bonding state of the hydroxyl group. Thus, we discount the 1.5-cm^{-1} Y8a band frequency shift and from our other data conclude that the Tyr-$\alpha_1$42 residue becomes more of an H-bond donor in the T state of metHbF.

The Trp Raman excitation profile red-shift suggests an increased H-bonding donation of Trp-β37 (Table 3). Trp-β37 should be more strongly H-bonded in the T state than in the R state since the basicity of the T-state H-bonding partner, the Asp-α94 carboxylate group, is larger than that of the R-state H-bonding partner, the Asn-β102 backbone carbonyl group. It should be noted that, based on comparison of the 230-nm excited UVRR difference spectrum of metHbF+IHP minus metHbF to that of deoxyHb minus HbCO, Jayaraman et al. (1993) recently suggested that IHP binding to metHbF only partially induces the T state, and the H-bonding interactions of the interior Trp-α14 and Trp-β15 residues are perturbed by tertiary strain in T-state metHbF+IHP. Our 229-nm excited UVRR difference spectrum of metHbF+IHP minus metHbF is simialr to their 230-nm excited UVRR difference spectrum; we also observed that the Trp 1360/1340-cm^{-1} band intensity ratio increases in the T state. This Trp W7 Fermi resonance doublet band around 1350 cm^{-1} is sensitive to the microenvironment of Trp (Chen et al., 1973; Yu, 1974; Harada et al., 1986), and the increased 1360/1340-cm^{-1} intensity ratio may result from an increased hydrophobicity of the Trp-β37 environment (Shaanan, 1983). However, this intensity ratio strongly depends on the UV excitation wavelength, and could change upon excitation profile shifts.

UVRR Saturation Behavior of Trp and Tyr Residues in Hemoglobin. The ratio of hemoglobin Trp and Tyr band intensities to that of the 607-cm^{-1} cacodylic acid band directly monitors the populations of ground-state species during each incident laser pulse. Recently our laboratory introduced Raman saturation spectroscopy (Harmon et al., 1990; Teraoka et al., 1990) as a technique to monitor the rate of photochemical relaxation to the ground state. We monitor the dependence of the Raman intensity of an absorbing sample upon the incident pulse energy flux density. The Raman intensity, which is directly proportional to the ground-state population, depends upon the absorption cross section, the lifetime of excited states, and the incident pulse energy flux. Using this model (Harmon et al., 1990; Teraoka et al., 1990), we determined the ground-state relaxation rates of Trp residues of human metHbF in both the R and T states to be $1/120 \pm 35$ ps. We also calculated identical Tyr R- and T-state T_1 relaxation rates of *ca.* $1/60 \pm 40$ ps. This faster Tyr relaxation rate presumably is the result of closer proximity of the Tyr residues to the hemes and to the Trp, permitting very efficient Tyr Förster energy transfer. The invariance of these relaxation rates on quaternary structural changes indicates that there is little alteration in the distance or orientation of the Tyr and Trp residues relative to the heme between the two quaternary structures and that Förster transfer to the heme probably dominates this relaxation behavior. The observed Trp T_1 rates are slower than those measured for the Trp residues of horse metmyoglobin, whose average value is 1/70 ps (Harmon et al., 1990).

All previous reports show that heme protein aromatic residue fluorescence is strongly quenched by the heme through Förster energy transfer (Hirsch et al., 1980; Hirsch & Nagel, 1981; Itoh et al., 1981; Szabo et al., 1984, 1989; Bucci et al., 1988a,b). Such energy transfer occurs over long distances because of overlap of the emission bands of the aromatic residues with the heme absorption bands. The Trp residue with the longest lifetime in Hb is ascribed to the β37 Trp residue which we also implicate as the residue whose Raman cross section changes.

We observe essentially no quaternary structural dependence for the metHbF Trp and Tyr relaxation rates. As far as we know, no direct fluorescence studies of metHbF in the R and T states exist. However, our results are consistent with measurements of the fluorescence lifetime of other Hb derivatives. Front-face fluorescence studies find multiexponential decays which resolve into three different relaxation rates of the order of 1/10–1/90 ps, 1/5 ns, and 1/1 ns which are identical for the R- and T-state quaternary structures (Szabo et al., 1989; Bucci et al., 1988a,b); the longer nanosecond component is believed to originate from the intrinsic fluorescence of the Trp-β37 residue based on mutant Hb studies (Hirsch & Nagel, 1981). Trp relaxation rates are significantly faster in Mb than in Hb (Hochstrasser & Negus, 1984).

CONCLUSIONS

We have observed absorption and resonance Raman excitation profile red-shifts for the metHbF Trp and Tyr residues upon the R–T quaternary structure change induced by the allosteric effector IHP. We ascribe these changes to alterations of the Trp-β37 and Tyr-α42 residue environments and hydrogen bonding states at the $\alpha_1\beta_2$ subunit interface. Our results suggest that the T-state Tyr-α42 residue donates rather than accepts an H-bond to the carboxyl group of Asp-β99. We also used Raman saturation spectroscopy to measure the electronic excited-state relaxation rates of the metHbF Tyr and Trp residues. These are identical for the R and T forms within the accuracy of our measurements. We observe relaxation times of 1/60 and 1/120 ps for the Tyr and Trp residues, respectively. The results for Trp are similar to those measured by front-face fluorescence. These Tyr relaxation measurements are the first measurements of Tyr excited-state relaxation in any heme protein.

We believe our study here is the first observation of an easily measured, strong absorption spectral change in the 230-nm region diagnostic of the environment of Trp and Tyr residues at the subunit interface. This absorption spectral change could be easily used to monitor the kinetics of the Trp–Tyr quaternary structural alterations. This absorption spectral change correlates with weaker absorption spectral changes in the *ca.* 280-nm spectral region previously assigned to Trp-β37 and Tyr-α42 residues.

ACKNOWLEDGMENT

We thank Dr. Wonghil Chang and Dr. Sung-mo Choi for technical help in synthesizing the model peptides and for NMR measurements. We thank Dr. William Gustafson and Mr. Stewart Getzow for help in the early stages of this work. We thank Professor Richard Day for help with statistical analysis and Dr. John Rose for help in setting up the protein structural data files for use with the molecular modeling program on a Silicon Graphics workstation. We thank Professor Andrew Hamilton, Dr. Brian Linton, and Mr. Jeffrey Albert for help in using SYBYL, the molecular modeling software.

REFERENCES

Albrecht, A. C. (1960) *J. Chem. Phys. 34*, 1476.

Albrecht, A. C., & Hutley, M. C. (1971) *J. Chem. Phys. 55*, 4438.

Antonini, E., & Brunori, M. (1971) *Hemoglobin and Myoglobin in Their Reactions with Ligands*, North-Holland Publishing, Amsterdam.

Asher, S. A. (1981) *Methods Enzymol. 76*, 371.

Asher, S. A. (1988) *Annu. Rev. Phys. Chem. 39*, 537.

Asher, S. A., & Schuster, T. M. (1981) *Biochemistry 20*, 1866.

Asher, S. A., Vickery, L. E., Schuster, T. M., & Sauer, K. (1977) *Biochemistry 16*, 5849.

Asher, S. A., Adams, M. L., & Schuster, T. M. (1981) *Biochemistry 20*, 3339.

Asher, S. A., Johnson, C. R., & Murtaugh, J. (1983) *Rev. Sci. Instrum. 54*, 1657.

Asher, S. A., Larkin, P., & Teraoka, J. (1991) *Biochemistry 30*, 5324.

Asher, S. A., Bormett, R. W., Chen, X. G., Lemmon, D. H., Cho, N., Peterson, P., Arrigoni, M., Spinelli, L., & Cannon, J. (1993) *Applied Spectrosc. 47*, 628.

Bailey, J. E., Beaven, G. H., Chignell, D. A., & Gratzer, W. B. (1968) *Eur. J. Biochem. 7*, 5.

Baldwin, J. M. (1975) *Prog. Biophys. Mol. Biol. 29*, 225.

Baldwin, J., & Chothia, C. (1979) *J. Mol. Biol. 129*, 175.

Bucci, E., Malak, H., Fronticelli, C., Gryczynski, I., Laczko, G., & Lakowicz, J. R. (1988a) *Biophys. Chem. 32*, 187.

Bucci, E., Malak, H., Fronticelli, C., Gryczynski, I., & Lakowicz, J. R. (1988b) *J. Biol. Chem. 263*, 6972.

Chen, M. C., Lord, R. C., & Mendelsohn, R. (1973) *Biochim. Biophys. Acta 328*, 252.

Cho, N., & Asher, S. A. (1993) *J. Am. Chem. Soc. 115*, 6349.

Copeland, R. A., & Spiro, T. G. (1987) *Biochemistry 26*, 2134.

Copeland, R. A., Dasgupta, S., & Spiro, T. G. (1985) *J. Am. Chem. Soc. 107*, 3370.

Dasgupta, S., Copeland, R. A., & Spiro, T. G. (1986) *J. Biol. Chem. 261*, 10960.

Deatherage, J. F., Loe, R. S., & Moffatt, K. (1976) *J. Mol. Biol. 104*, 723.

Demchenko, A. P. (1981) *Ultraviolet Spectroscopy of Proteins*, Chapter 2, p 27, Springer-Verlag, Berlin.

Dickerson, R. E., & Geis, I. (1983) *Hemoglobin*, Benjamin Cummings Publishing, Menlo Park, CA.

Eaton, W. A., & Hochstrasser, R. M. (1970) *J. Chem. Phys. 49*, 985.

Fermi, G., & Perutz, M. F. (1977) *J. Mol. Biol. 114*, 421.

Fodor, S. P. A., & Spiro, T. G. (1986) *J. Am. Chem. Soc. 108*, 3198.

Harada, I., & Takeuchi, H. (1986) in *Spectroscopy of Biological Systems* (Clark, R. J. H., & Hester, R. E., Eds.) p 113, John Wiley & Sons, Chichester, U.K.

Harada, I., Miura, T., & Takuechi, H. (1986) *Spectrochim. Acta, Part A 42*, 307.

Harmon, P. A., & Asher, S. A. (1988) *J. Chem. Phys. 88*, 2925.

Harmon, P. A., & Asher, S. A. (1990) *J. Chem. Phys. 93*, 3094.

Harmon, P. A., Teraoka, J., & Asher, S. A. (1990) *J. Am. Chem. Soc. 112*, 8789.

Heidner, E. J., Ladner, R. C., & Perutz, M. F. (1976) *J. Mol. Biol. 104*, 707.

Henry, E. R., Rousseau, D. L., Hopfield, J. J., Noble, R. W., & Simon, S. R. (1985) *Biochemistry 24*, 5907.

Hirsch, R. E., & Nagel, R. L. (1981) *J. Biol. Chem. 256*, 1080.

Hirsch, R. E., Zukin, R. S., & Nagel, R. L. (1980) *Biochem. Biophys. Res. Commun. 93*, 432.

Hochstrasser, R. M., & Negus, D. K. (1984) *Proc. Natl. Acad. Sci. U.S.A. 81*, 4399.

Itoh, M., Mizukoshi, H., Fuke, K., Matsukawa, S., Mawatari, K., Yoneyama, Y., Sumitani, M., & Yoshihara, K. (1981) *Biochem. Biophys. Res. Commun. 100*, 1259.

Jayaraman, V., Rodgers, K. R., Mukerji, I., & Spiro, T. G. (1993) *Biochemistry 32*, 4547.

Johnson, C. R., Ludwig, M., O'Donnell, S., & Asher, S. A. (1984) *J. Am. Chem. Soc. 106*, 5008.

Johnson, C. R., Ludwig, M., & Asher, S. A. (1986) *J. Am. Chem. Soc. 108*, 905.

Jones, C. M., De Vito, V. L., Harmon, P. A., & Asher, S. A. (1987) *Appl. Spectrosc. 41*, 1268.

Kaminaka, S., & Kitagawa, T. (1992) *J. Am. Chem. Soc. 114*, 3256.

Kaminaka, S., Ogura, T., & Kitakawa, T. (1990) *J. Am. Chem. Soc. 112*, 23.

Kamlet, M. J., Abboud, G. L. M., & Taft, R. W. (1981) *Prog. Phys. Org. Chem. 13*, 485.

Ladner, R. C., Heidner, E. J., & Perutz, M. F. (1977) *J. Mol. Biol. 114*, 385.

Larkin, P. J., Gustafson, W. G., & Asher, S. A. (1991) *J. Chem. Phys. 34*, 5324.

Ludwig, M., & Asher, S. A. (1988) *J. Am. Chem. Soc. 110*, 1005.

Noble, R. W., De Young, A., & Rousseau, D. L. (1989) *Biochemistry 28*, 5293.

Painter, P. C., & Koenig, J. L. (1976) *Biopolymers 15*, 241.

Perutz, M. F. (1979) *Annu. Rev. Biochem. 48*, 327.

Perutz, M. F., Ladner, J. E., Simon, S. R., & Ho, C. (1974a) *Biochemistry 13*, 2163.

Perutz, M. F., Fersht, A. R., Simon, S. R., & Roberts, G. C. K. (1974b) *Biochemistry 13*, 2174.

Perutz, M. F., Heidner, E. J., Ladner, J. E., Beetlestone, J. G., Ho, C., & Slade, E. F. (1974c) *Biochemistry 13*, 2187.

Perutz, M. F., Sanders, J. K. M., Chenery, D. H., Noble, R. W., Pennelly, R. R., Fung, L. W.-M., Ho, C., Giannini, I., Porschke, D., & Winkler, H. (1978) *Biochemistry 17*, 3640.

Perutz, M. F., Fermi, G., Luisi, B., Shaanan, B., & Liddington, R. C. (1987) *Acc. Chem. Res. 20*, 309.

Pezolet, M., Yu, T.-J., & Peticolas, W. L. (1975) *J. Raman Spectrosc. 3*, 55.

Rodgers, K. R., Su, C., Subramaniam, S., & Spiro, T. G. (1992) *J. Am. Chem. Soc. 114*, 3697.

Rousseau, D. L., & Ondrias, M. R. (1983) *Annu. Rev. Biophys. Bioeng. 12*, 357.

Rousseau, D. L., & Friedman, J. M. (1988) *Biological Applications of Raman Spectroscopy* (Spiro, T. G., Ed.) Vol. III, Chapter 4, p 113, John Wiley & Sons, New York.

Shaanan, B. (1983) *J. Mol. Biol. 171*, 31.

Smith, D. W., & Williams, R. J. P. (1970) *Struct. Bonding (Berlin) 7*, 1.

Song, S., & Asher, S. A. (1989) *J. Am. Chem. Soc. 111*, 4295.

Song, S., & Asher, S. A. (1991) *Biochemistry 30*, 1199.

Song, S., Asher, S. A., Krimm, S., & Shaw, K. D. (1991) *J. Am. Chem. Soc. 113*, 1155.

Spiro, T. G., & Strekas, T. C. (1974) *J. Am. Chem. Soc. 96*, 338.

Spiro, T. G., Smulevich, G., & Su, C. (1990) *Biochemistry 29*, 4497.

Su, C., Park, Y. D., Liu, G.-Y., & Spiro, T. G. (1989) *J. Am. Chem. Soc. 111*, 3457.

Sweeney, J. A., & Asher, S. A. (1990) *J. Phys. Chem. 94*, 4784.

Sweeney, J. A., Harmon, P. A., Asher, S. A., Hutnik, C. M., & Szabo, A. G. (1991) *J. Am. Chem. Soc. 113*, 7531.

Szabo, A. G., Krajcarski, D., Zuker, M., & Albert, B. (1984) *Chem. Phys. Lett. 108*, 145.

Szabo, A. G., Krajcarski, D. T., & Albert, B. (1989) *Chem. Phys. Lett. 163*, 565.

Takeuchi, H., Watanabe, N., Satoh, Y., & Harada, I. (1989) *J. Raman Spectrosc. 20*, 233.

Takeuchi, H., Ohtsuka, Y., & Harada, I. (1992) *J. Am. Chem. Soc. 114*, 5321.

Teraoka, J., Harmon, P. A., & Asher, S. A. (1990) *J. Am. Chem. Soc. 112*, 2892.

Viggiano, G., & Ho, C. (1979) *Proc. Natl. Acad. Sci. U.S.A. 76*, 3673.

Yu, N. T. (1974) *J. Am. Chem. Soc. 96*, 4664.